

Final Technical Report

Development of a Holocene earthquake record for the northern Agua Tibia-
Earthquake Valley Fault Zone from a new paleoseismic site at Warner Basin :
Collaborative Research with UCI and SDSU

Thomas K. Rockwell

Department of Geological Sciences

San Diego State University

5500 Campanile Dr.

San Diego, CA 92182-1020

P: (619) 594-4441, trockwell@mail.sdsu.edu

Award Number G12AP20070

Sinan Akciz

Earth, Atmospheric and Planetary Sciences,

University of California, Los Angeles

595 Charles Young drive East, Los Angeles, CA 90095

Award Number G13AP00060

July, 2014

Abstract

We report the results of new mapping, dating and paleoseismic work along the Agua Tibia – Earthquake Valley fault zone, hereafter referred to as simply the Earthquake Valley fault, in Warner Basin, San Diego County, southern California. The fault is well expressed as a narrow zone of aligned scarps, springs, vegetation lineaments and sag features in Warner Basin, which is filled with middle Quaternary deposits that contain the Bishop Tuff. We dated the tuff in Warner Basin to about 790 ka, confirming its correlation to the widespread tephra. The margins of the basin are offset about 1.9 km, as is the main axial channel that incises the basin deposits. Together, we estimate that the long-term slip rate for the Earthquake Valley fault in this area is about 2.5 mm/yr, which is similar to that assigned to the Elsinore fault near Julian.

We excavated two trenches in Big Lake, a shallow closed depression that we interpret as a sag feature along the fault. The stratigraphy at the site is reasonably good, with stratified, generally fine-grained sediments, and a single but discontinuous shallow peat-like horizon in the upper meter. The presence of abundant charcoal allows for a fairly precise characterization of the chronology of sediment deposition, which indicates that the upper 2.5 m of section was deposited in the past 2.6 ka. The upper half-meter contained a 1950's vintage shotgun shell, indicating that rapid sedimentation has continued into the historical period.

The fault is expressed as a broad zone with numerous small fractures and fault strands, consistent with the interpretation that Big Lake is a structural depression. We identified three horizons up to which there is evidence of coeval shattering and displacement on many of the fault strands. The uppermost interpreted event breaks up to within 20 cm of the historical horizon and suggests a very young surface rupture. Based on the sequence of dates, we possibly attribute this event (E1) to the 1890 earthquake, which was moderate (M6.5 range) in size but only recorded at distance locations. The two earlier interpreted events date to about 800 AD and 0 AD, suggesting a recurrence interval of about 900-1000 years.

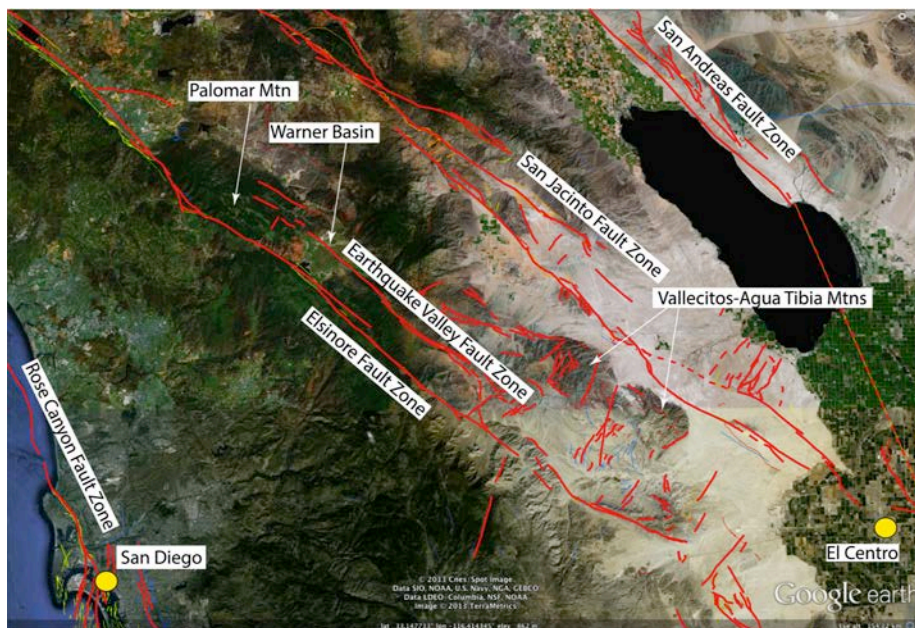


Figure 1.

Introduction

The Agua Tibia - Earthquake Valley fault zone, hereafter referred to as the Earthquake Valley, fault is considered the eastern strand of the Elsinore fault zone in southern California (Magistrale and Rockwell, 1996). The Earthquake Valley fault is sub-parallel to the Elsinore fault, which is simpler and single

stranded to the north of Temecula and south of the Tierra Blanca Mountains (Figure 1). The Agua Tibia-Palomar Mountain uplift is interpreted to be a large pressure ridge system that steps part of the north Elsinore slip to the southeast onto the Earthquake Valley fault. The Earthquake Valley fault is interpreted to transfer this component of deformation back to the southern San Jacinto fault zone via another restraining step at the Vallecito-Fish Creek Mountains, a topographic bedrock high bounded by deep alluvial fill.

In this paper, we briefly describe the geomorphology along the Earthquake Valley fault in Earthquake Valley and Warner Basin, and describe the offset of Warner Basin and its associated alluvial fill, which we use to estimate the long-term slip rate. We then present our new paleoseismic results on the late Holocene activity of the Earthquake Valley fault at Big Lake in Warner Basin.

Tectonic Geomorphology

The earthquake Valley fault is well expressed in the geomorphology from Earthquake Valley northwest through Warner Basin. Magistrale and Rockwell (1996) described clear geomorphic indicators of right-lateral slip in Earthquake Valley, as well as delineated the discrete double-zoned nature of the seismicity along the Elsinore fault system through this region. In their work, Magistrale and Rockwell (1996) used vintage (1953) aerial photography to locate and describe geomorphic features indicative of young motion. With the advent of Google Earth, it is now possible to rapidly map such features along active faults, and we have reassessed the geomorphology in Earthquake Valley, as well as extended the earlier work to the northwest through Warner Valley. In this section, we first briefly re-describe the geomorphology in Earthquake Valley and follow with new descriptions of the fault in Warner Valley.

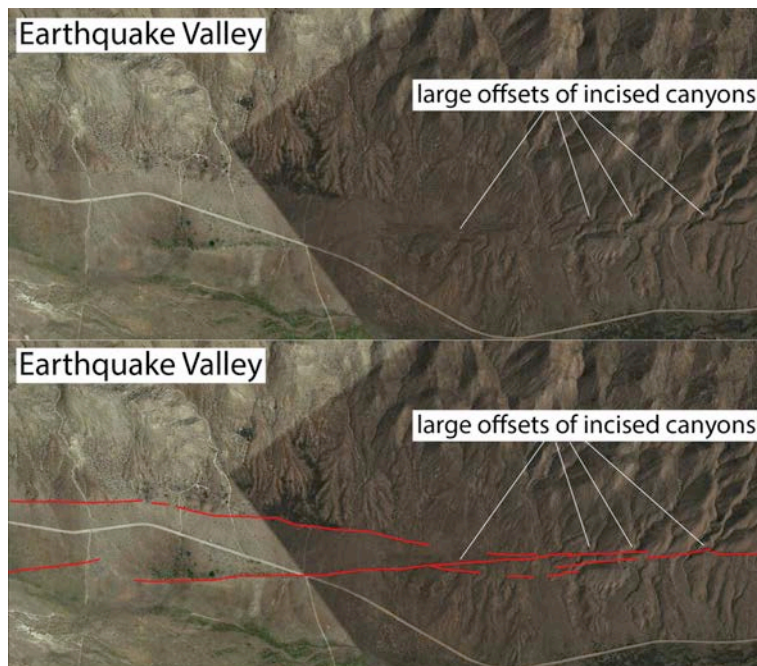


Figure 2. Geomorphic expression of the Earthquake Valley fault in Earthquake Valley. Note the large deflections of drainages incised into Pleistocene alluvial fan deposits.

Earthquake Valley Section – The fault is very well-expressed along the hills that flank the northeast side of Earthquake Valley north of highway 78, where drainages incise Pleistocene alluvial fans. Along this section of fault, there are numerous examples of offset and beheaded drainages, scarps, deflections, vegetation lineaments, side-hill benches, and other examples of the presence and activity of the fault (Figures 2 and 3). Many of the major drainages exhibit large deflections, and some drainages are beheaded. Figure 4 shows plausible reconstructions for drainages incised into two levels or ages of Pleistocene alluvial fan deposits. Future work will focus

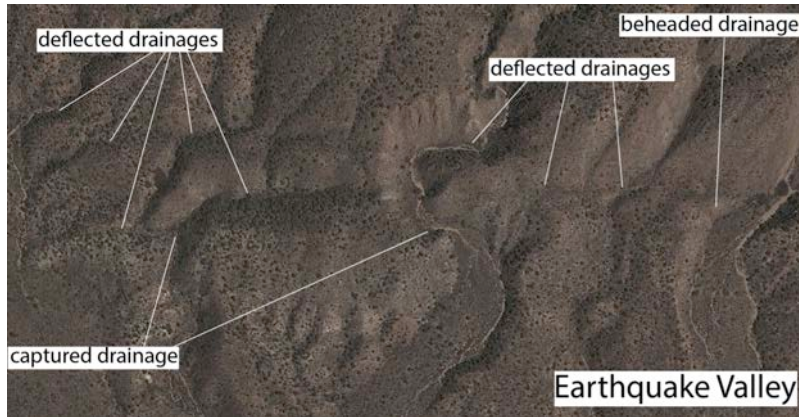


Figure 3. Detail of deflected, captured and beheaded drainages in Earthquake Valley north of Highway 78 and northeast of Highway S2.

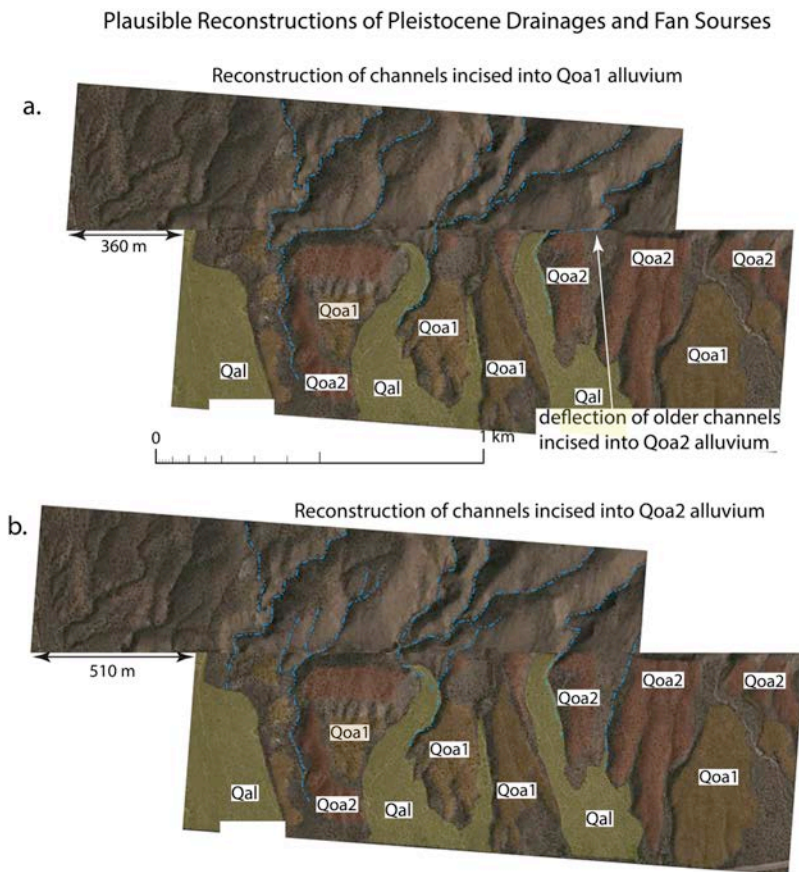


Figure 4. Plausible reconstructions of major drainages that incise late Pleistocene alluvial fan deposits. In a), reconstruction of 360 m aligns drainages that incise the Qoa1 deposits, whereas in b), 510 m of reconstruction realign drainages that incise the Qoa2 deposits. None of these deposits have yet been dated.

on the ages of these deposits to better resolve the late Quaternary slip rate in Earthquake Valley.

To the southeast of Highway 78, the Earthquake Valley fault exhibits good expression within the alluvial fan bajada along the northeast margin of “Shelter Valley” (Figure 5). The geomorphology along this stretch of fault is considerably younger than to the north in Earthquake Valley but the location of the fault is clearly discernable as scarps in late Pleistocene and Holocene fan deposits, and as vegetation lineaments (Figure 5). A minor secondary strand is interpreted in the hills to the northeast, as shown by a dashed lined in Figure 5.

To the southeast of Shelter Valley, the fault zone is not well-expressed as a single main trace. There are many northeast-striking left lateral faults, along with several minor northwest-striking right-lateral faults (Gordon and Rockwell, 2013). Further, the Vallecitos-Fish Creek Mountain uplift, which we interpret as a pressure ridge system resulting from the stepping of slip from the Earthquake Valley fault southeast to the southern San Jacinto fault zone.

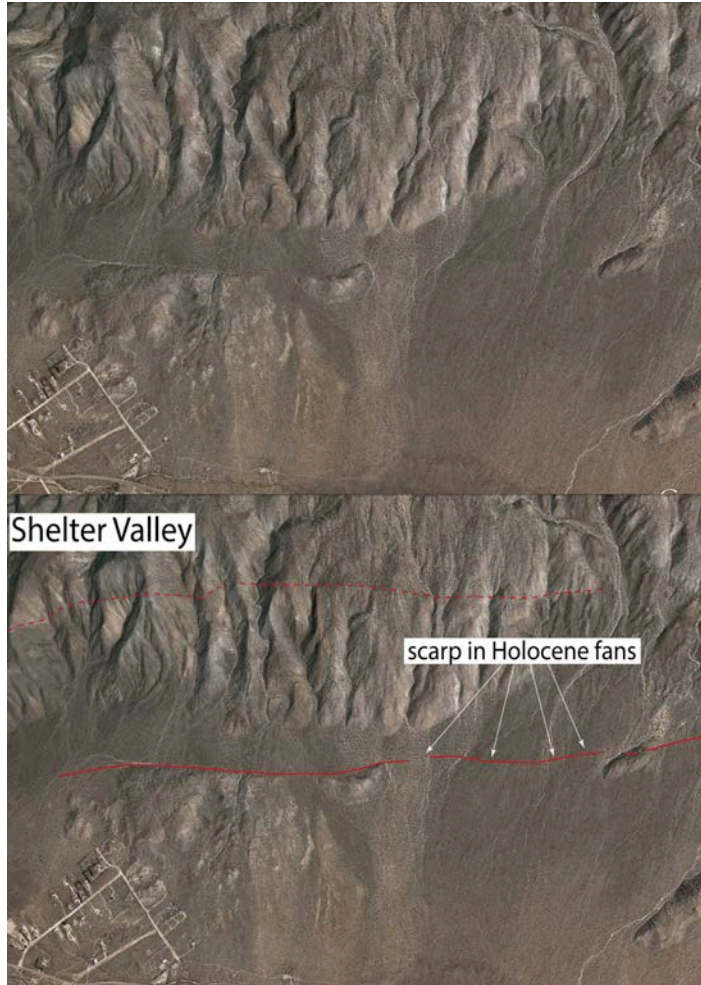


Figure 5. Location of the Earthquake Valley fault in “Shelter Valley” south of Highway 78, as expressed as scarps and vegetation lineaments in late Quaternary alluvial fan deposits.



Figure 6. The Earthquake Valley fault in Warner Basin, as viewed to the southeast in Google Earth imagery.

Warner Basin Section – The fault in Warner Basin is also well-expressed but exhibits quite different geomorphic features, because the fault is generally limited to the valley bottom and appears to exhibit a nearly pure strike-slip sense of displacement. Figure 6 is an oblique Google EarthPro image looking to the southeast along the fault, which is expressed as a linear array of scarps, pressure ridges at small left bends or steps, a fossil sag pond that is apparent offset along the currently active trace, and Big Lake, a closed depression that we interpret as an active sag feature. A tonal lineament across Big Lake suggested to us that the fault is still relatively localized and may be fruitful for paleoseismic study, as discussed below.

Figure 7 shows a more detailed image of the fault zone in Warner Valley, with the interpreted main strand, along with secondary strands. The tonal lineament in Big Lake is clearly visible, and the trench site is indicated, as discussed below. A significant secondary strand appears to be present to the north of the primary strand and is aligned with springs. The high water table along this strand precluded sub-surface work, although it is likely that fine-grained stratigraphy and associated peat-like layers are present.

To the northwest of Warner Basin, the fault appears to splay into multiple strands in the Palomar Mountain region, which we interpret is due to the stepping of lateral



Figure 7. The Earthquake Valley fault across the central portion of Warner Basin, as viewed in a Google Earth image. The blue triangles indicate the location of the main or primary strand, as interpreted because of the strength of its expression. The yellow triangle indicate the location of a significant secondary strand that appears to control ground water to some extent, and has significant spring activity aligned with it. The magenta triangles indicate the possible presence of a third fault strand. The location of the paleoseismic work is indicated by the trench in Big Lake.

displacement to the west to the northern Elsinore fault. The fault strands in the Palomar-Agua Tibia Mountain uplift are discontinuous in their expression and no strand appears to exhibit the same strength of geomorphic character as observed in Warner Basin or Earthquake Valley. This is similar to the loss of expression of the fault zone southeast of Shelter Valley, so the well-expressed part of the Earthquake Valley fault zone is limited to Warner Basin southeast through Shelter Valley.

Estimation of the Slip Rate at Warner Basin

Warner Basin lies to the southeast of Palomar Mountain (Figure 1 and 8) and is actually more a filled valley than a structural basin. The valley fill deposits are on the order of a few tens of meters in thickness and likely resulted from blockage of the outflow channel, the San Luis Rey River. The age of the valley fill has been inferred to be middle Quaternary based on the presence of a tephra that is correlated to the Bishop Tuff (Merriam and Bischoff, 1975). We located an outcrop of the tuff and collected it for isotopic dating to confirm its age and correlation to the Bishop Tuff, as discussed below.

The valley fill deposits of Warner Basin, along with the axial drainage that bisects these deposits, appears to be offset about 1.9 km in a right-lateral sense (Figure 8). Although the margins of the basin could have exhibited some offset prior to deposition of the valley fill, thereby giving the appearance that the deposits are offset by the full amount, we consider it

unlikely that the axial drainage that incises the deposits would show the same amount of deflection unless the 1.9 km of apparent offset represents the actual displacement of the fill. Thus, we interpret the 1.9 km right deflection of the valley fill margins and axial drainage to represent displacement after deposition of the alluvial fill.

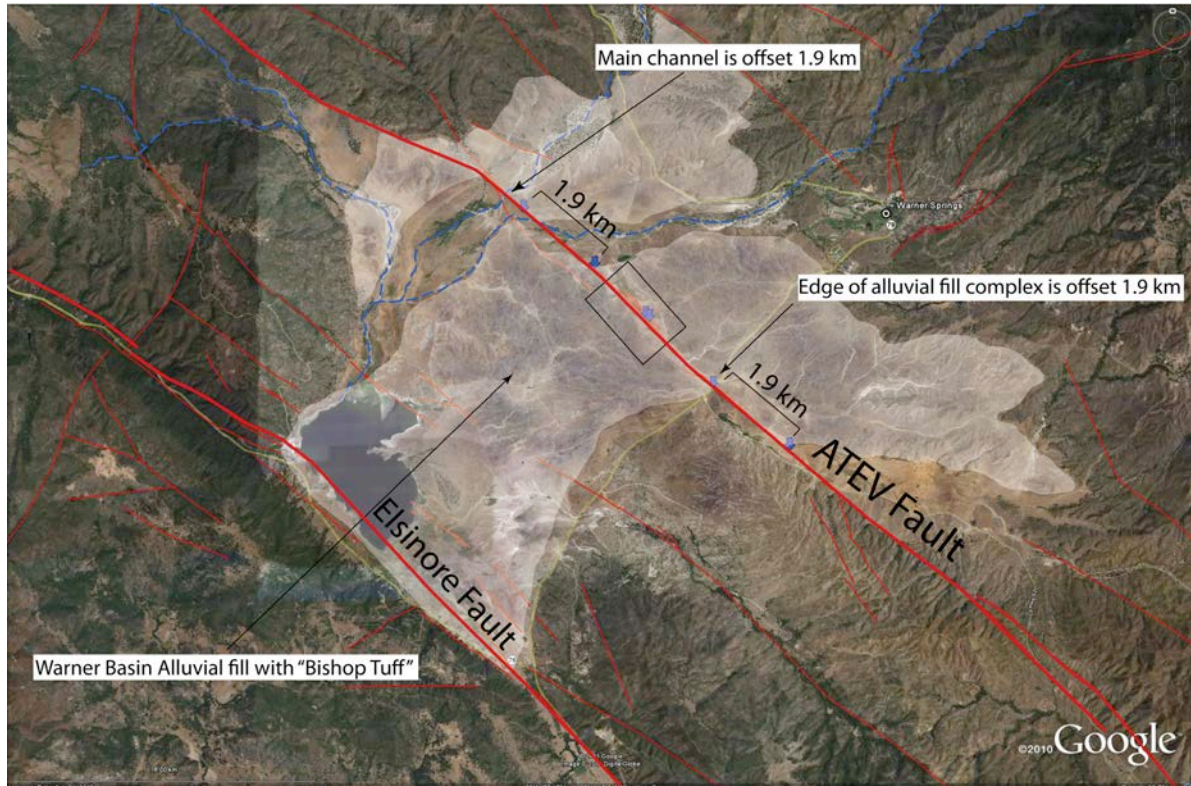


Figure 8. Map of middle Quaternary alluvial deposits in the Warner Basin that contain the Bishop Tuff (780 ka). Note that the SE margin of these basin deposits is offset 1.9 km, as is the major drainage system that flows through the basin deposits. We will map subunits of these deposits to confirm this offset, which yields a long-term rate of about 2.5 mm/yr.

Secondary Ionization Mass Spectrometry (SIMS) Zircon Geochronology - Zircons were separated from the tephra using cold HF (40%) digestion of glass followed by heavy mineral separation using methylene iodide at a nominal density $\rho = 3.3 \text{ g/cm}^3$. After hand-picking of euhedral crystals, zircons were embedded in epoxy resin and gently abraded to expose crystal interiors. Analysis of U-Pb isotopes followed procedures described in Schmitt et al. (2003). All ages are reported relative to reference zircon AS3 with an age of 1099.1 Ma (Paces and Miller, 1993). Because of the young age of most zircon crystals in the sample, a correction for ^{230}Th disequilibrium was performed assuming that the initial abundance of ^{230}Th zircon was only 20% of the equilibrium abundance. This correction adds ca. 90 ka to the equilibrium $^{206}\text{Pb}/^{238}\text{U}$ age. Nine out of 10 analyzed zircons yielded Quaternary ages (after correction for ^{230}Th disequilibrium), which averaged $790 \pm 26 \text{ ka}$ (mean square of weighted deviates MSWD = 0.5; 2σ error) (Figure 9). A single older ($93.9 \pm 7.8 \text{ Ma}$) crystal was encountered. Zircon

xenocrysts are rare in Bishop Tuff (e.g., Reid and Coath, 2000; Simon et al., 2005; Chamberlain et al., 2014), and it is therefore tentatively concluded that this crystal is of detrital origin. Otherwise, the remaining zircon population agrees within uncertainty with published SIMS ages for Bishop Tuff zircon from proximal (Reid and Coath, 2000; Simon et al., 2005; Chamberlain et al., 2014) and distal locations (Schmitt and Hulen, 2008). Moreover, U abundances in zircons from the tephra in Warner Basin are elevated for the Bishop Tuff aged zircons (~1600-5600 ppm), which is characteristic for zircon from early-erupted Bishop Tuff. Based on the close zircon age overlap and similarity in composition, the tephra in Warner Basin is confidently identified as the Bishop Tuff. Because zircon crystallizes prior to eruption, the $^{206}\text{Pb}/^{238}\text{U}$ zircon overestimates the depositional age for the ash, which based on recent determinations is pegged between 767.4 ± 0.2 ka (Rivera et al., 2011) and 781 ± 2 ka (Simon et al., 2014), consistent with our new date.

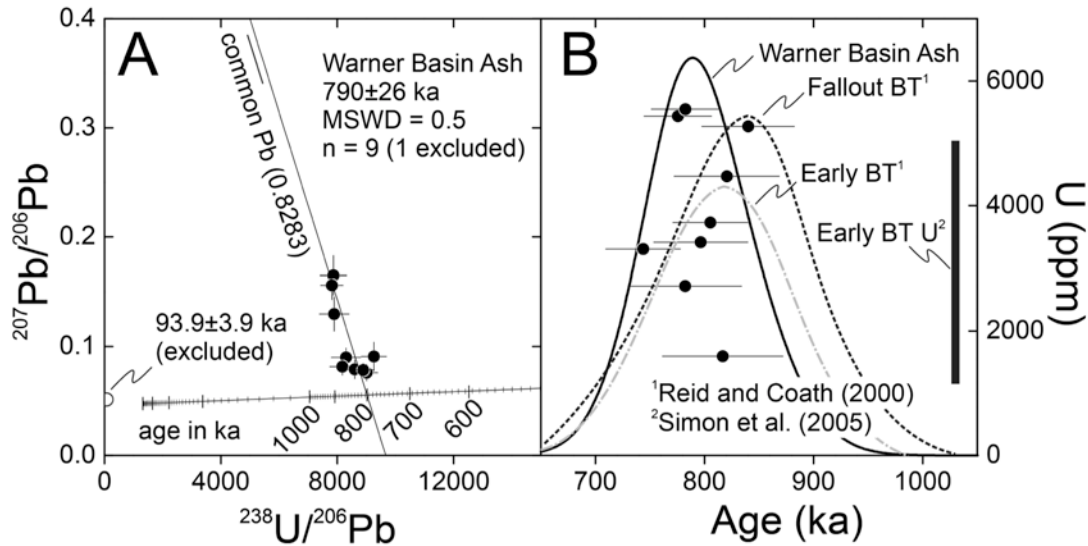


Figure 9. Zircon geochronology results for Elsinore ash. (A) $^{207}\text{Pb}/^{206}\text{Pb}$ vs. $^{238}\text{U}/^{206}\text{Pb}$ concordia diagram with age intervals (large ticks) of 100 ka adjusted for ^{230}Th disequilibrium. Data are plotted uncorrected for common Pb together with regression line with fixed y-axis intercept corresponding to common $^{207}\text{Pb}/^{206}\text{Pb} = 0.8283$. (B) U abundance vs. $^{206}\text{Pb}/^{238}\text{U}$ age and relative probability of zircon ages in comparison to proximal Bishop Tuff zircon ages (Reid and Coath, 2000) and U-abundances (Simon et al., 2005).

Slip Rate – We calculate the long-term slip by taking the inferred offset of 1.9 km and dividing by the 790 ± 26 ka age we determined for the Bishop Tuff in Warner Basin. Using the minimum and maximum age constraints and a ~10% uncertainty for displacement (1.9 ± 0.2 km) yields a rate of $2.53^{+0.22}_{-0.45}$ mm/yr, which we round up to $2.5^{+0.3}_{-0.5}$ mm/yr. This rate is a minimum because the tephra is older than the capping surface into which the axial channel is incised, but the age difference is probably well within the stated uncertainties, so we take this as a fair representation of the long-term rate for the Earthquake Valley fault in Warner Basin. If we use the best estimates for the age of the Bishop Tuff (767.4 ± 0.2 ka (Rivera et al., 2011) and

781±2 ka (Simon et al., 2014)), assuming that the Warner Basin tephra is the Bishop Tuff as we infer, then the rate drops by a few percent, well within our estimates of uncertainty.

Paleoseismology at Big Lake

We excavated two parallel trenches across the tonal lineament (Figures 6 and 7) at Big Lake with the intent of studying the timing of past surface ruptures along the Earthquake Valley fault in Warner Basin. The site was chosen because initial 1 m-deep auger borings indicated the presence of a shallow peak-like horizon, and because the stratigraphy in the upper meter looked promising. The stratigraphy at depth turned out to be less well-stratified than the upper meter, but was sufficient to identify faulted strata and evidence for past surface ruptures. Due to relatively high groundwater, we concentrated our efforts on the trench with the best stratigraphy and clearest faulting relationships, which we designate as trench T-1, the location of which is shown on Figure 7.

The fault through Big Lake is generally expressed as a broad zone of shattering, with many minor fault strands (Figures 10). A major fault was encountered at about 2 m depth, and apparently was activated during an earlier event, as discussed below, but not in the most recent event. The recent events are represented by numerous small faults that rupture up to two discrete horizons that we interpret as the surface at the time of the rupture. The evidence for each interpreted rupture is described in detail below, after a description of the stratigraphy. We should note that there are also numerous very minor cracks throughout the section that do not appear to have any coherence in terms of event horizons or common rupture levels. These may be due to ground shatter, water withdrawal, or possibly fault creep, although we do not see any other evidence for creep.

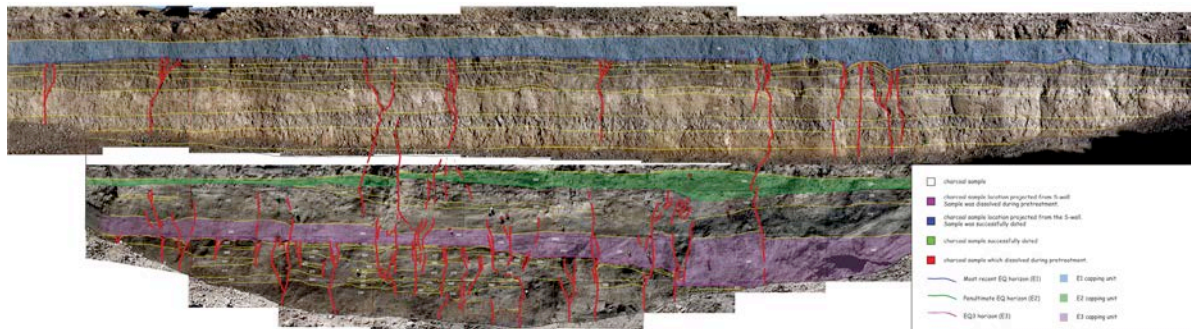


Figure 10. Log of the northwest wall of trench T1 at Big Lake. A bench separates the two portions of the log. The blue stratum is unit 50, which caps many filled fissures associated with event E1. Similarly, the green-colored stratum is unit 280, which caps faults that broke in event E2, and the purple-colored stratum is unit 390, that along with unit 400, caps fissures and faults that broke in event E3. Details are shown in figures 13, 14 and 15.

Description of Site Stratigraphy – We recognize more than 20 discrete and traceable units in the upper 2.5 m of section at Big Lake, which are summarized in Table 1 and described briefly below. Units 20 and 50 are clayey silt strata that are distinguished by their color and structure. Unit 20 contained a shotgun shell, indicating that it is historical in age and, based on the character of the shotgun shell, likely was deposited in the 1950's. Unit 90 is a dark gray silt horizon that we interpret as a weakly-form A or topsoil horizon based on its color and the presence of abundant fossil rootlets.

Table 1. *Big Lake T1 Unit Descriptions Based on N-Wall Observations*

Unit label	Description
20	Olive gray clayey silt; moderate subangular blocky structure; many roots; scattered snail shells; clear smooth boundary to unit 50.
50	Dark olive gray clayey silt; angular blocky structure; common to many roots; clear to abrupt (~2 cm) boundary to 90.
90	Dark gray silt; interpreted as a weak A-horizon; subangular blocky structure; abrupt boundary to 100; common to many roots.
100	Oxidized silt w/ fragments of 1-3 mm silt fragments; it may represent a burned surface; abrupt lower boundary above a peat-like, 1 cm thick organic unit that caps unit 110.
110	Highly organic dark gray to black silt w/ minor clay; moderate subangular blocky structure; abrupt lower contact; common roots.
130	Dark gray colored clayey silt; moderate subangular blocky structure; clear abrupt lower boundary; common roots.
150	Gray silt w/ minor clay & sand; moderate subangular blocky structure; common roots; abundant shells; clear to abrupt lower contact.
170	Olive gray fine silt; well-sorted; weak subangular blocky structure; secondary calcium carbonate on ped faces and in pores; clear lower contact.
190	Same as 170. Color is brownish-gray. Has much less carbonate. Clear to abrupt lower contact.
200	Light gray clayey silt w/ moderate to strong subangular to angular blocky structure; common roots; clear to abrupt lower contact.
250	Light brown clayey-silt w/ oxidation on ped faces; moderate subangular blocky structure, few roots, numerous root casts.
260	Like 250, but blockier
280	Laminated silt w/ 1-2 mm laminations defined by mica on parting surface
290	Brown clayey silt; moderate sub-angular blocky structure; abrupt boundary
300	Dark gray silty clay; organic enriched; interpreted as buried A-horizon. Moderate sub-angular to angular blocky structure.
350	Gray, clayey silt. Massive when moist.
390	Gray massive silty, clayey-silt. Pond sediment.
400	Gray clay, locally oxidized
410	Oxidized pebbly sand, 1-2 cm thick. Abrupt contacts. Distinct ringer unit.
440	Gray clay
450	Oxidized clayey silt
470	Gray clay
500	Weak A-horizon developed on 550
550	Dark gray saturated sandy, silty, clay w/ pebbles

Unit 100 is an oxidized silt layer with 1-3 mm-sized silt fragments or rip-ups that overlies a 1 cm-thick organic unit that caps unit 110. Unit 110 is a highly organic dark gray to black clayey silt with common roots, moderately formed soil structure and abrupt lower boundary, which we interpret as a well-formed buried A or topsoil horizon. Altogether, we interpret units

100-110 as a soil that likely experienced a surface burn, resulting in the surface oxidation observed for unit 100.

Units 130 down to 290 are moderately well stratified and laterally continuous that are dominated by silt, with some units exhibiting more sand and some with more clay. Of note, unit 170 exhibits secondary calcium carbonate on ped faces and in pores and is a marker unit that is

continuous on both walls. The carbonate likely accumulated during a dry period due to evaporative sapping, although the accumulation of some pedogenic carbonate cannot be ruled out.

Unit 300 is a dark gray silty clay with abundant organic matter and moderately developed soil structure that we interpret as another buried A soil horizon. Unit 300 caps a stratified sequence of silt layers interbedded with sand and clay layers. Unit 410 is a distinct, oxidized, well-sorted pebbly sand with abrupt contacts that could be correlated on both walls and traced the length of the trench until it dropped below the base of the trench on the northeast side of the main fault zone.

Altogether, the stratigraphy is reasonably well defined in both walls, and several of the units were distinct enough to allow certain correlation of units from one wall to the other.

Age of Units – We found abundant detrital charcoal fragments distributed throughout the section such that we have some age control on most units. As expected with detrital charcoal, some fragments yielded dates that are older than others from the same unit, and some dates are out of stratigraphic sequence. As a radiocarbon date represents the age of growth and death of annual rings in most trees, or perhaps single year growths if derived from seeds or cones, some range of ages are expected in any stratigraphic unit, with the possibility that some dates may be considerably older than others, and that all detrital charcoal dates are older than the host sediment unless introduced by bioturbation or some other process after sediment deposition. Hence, we have constructed our age model based on the assumption that the youngest dates from each unit represent the closest ages to the actual age of the unit. Although we cannot preclude that some charcoal was introduced at a later time, we were careful not to collect any samples that were found in krotovina (filled animal burrows), with the exception

Big Lake Trench 1 Samples

unit label	sample label	age	±error
50	2012BL1-31	dissolved	
	2012BL1-32	dissolved	
	2012BL1-33	dissolved	
	2012BL1-35		
	2012BL1-36	dissolved	
	2012BL1-45	dissolved	
E1			
90	2012BL1-26a		
	2012BL1-34	165	15
	2012BL1-39	dissolved	
	2012BL1-41	dissolved	
	2012BL1-50	dissolved	
100	2012BL1-3	dissolved	
	2012BL1-38	dissolved	
110	2012BL1-40	145	15
	2012BL1-43		
	2012BL1-44		
110/130 contact	2012BL1-1	115	15
	2012BL1-2	85	15
	2012BL1-5		
130	2012BL1-29	370	15
	2012BL1-42	dissolved	
150	2012BL1-27	340	15
	2012BL1-28		
	2012BL1-47		
190	2012BL1-37	620	15
	2012BL1-46		
250	2012BL1-4	915	20
	2012BL1-30	2120	80
280	2012BL1-21	not enough sample to pick	
	2012BL1-48	not enough sample to pick	
	2012BL1-49		
E2			
	2012BL1-20	dissolved	
340	2012BL1-16		
350	2012BL1-8	not enough sample to pick	
	2012BL1-9	not enough sample to pick	
	2012BL1-11	1690	20
	2012BL1-12	1665	15
	2012BL1-14	2035	45
	2012BL1-15	1565	20
	2012BL1-22		
	2012BL1-25		
390	2012BL1-17	2155	15
	2012BL1-18	1760	15
	2012BL1-19	not enough sample to pick	
	2012BL1-23	dissolved	
400	2012BL1-7	1825	25
E3			
450	2012BL1-13		
	2012BL1-26b		
550	2012BL1-6	2120	20
	2012BL1-10		
	2012BL1-24	2495	15

Table 2. C14 samples collected from trench T1. Note that many samples dissolved upon pretreatment, resulting in no age determination.

of buried A horizons, which are, by their very nature, thoroughly mixed and assumed to represent an age range during their periods of formation.

Altogether, we collected 51 samples for potential dating, of which we submitted 32 for dating, and for which 18 samples yielded dates (Table 2). Nearly half of the samples did not survive the acid-base-acid pretreatment. Of the samples that yielded ages, 14 samples were

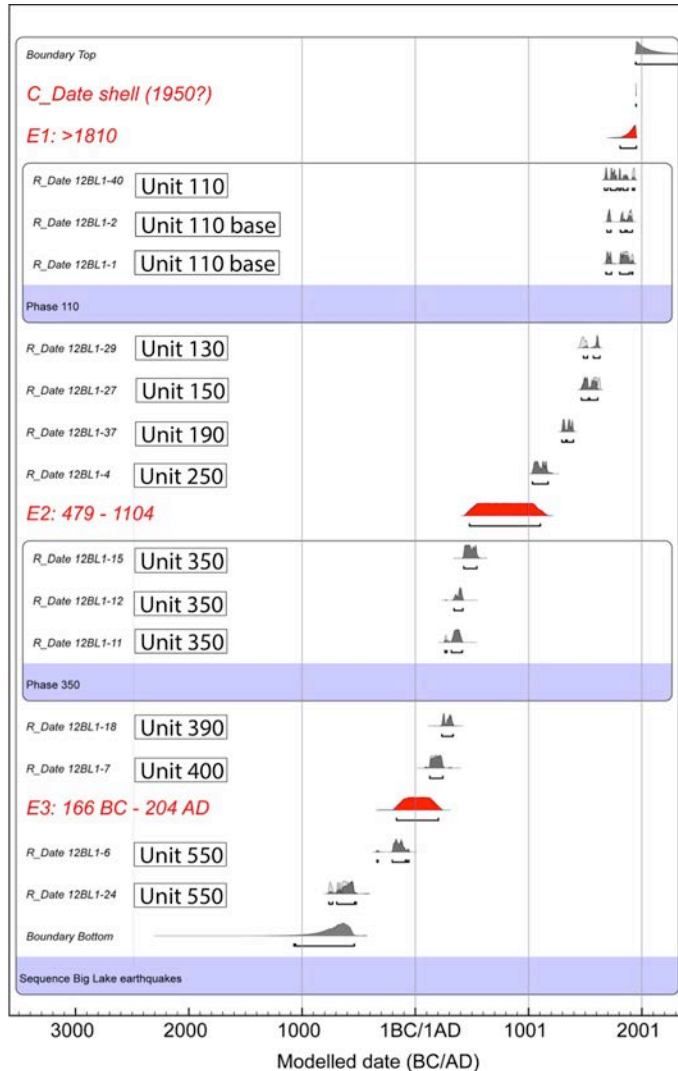


Figure 11. Chronologic model for the sediment history at Big Lake. All radiocarbon dates that do not violate the stratigraphic ordering are shown, as are the ages of the interpreted surface ruptures (in red).

next section, we discuss the evidence for each of our interpreted surface ruptures and place them in this chronology.

Interpreted Surface Ruptures – We have interpreted the occurrence of three surface ruptures at Big Lake over the past 2600 years or so, as recorded in the stratigraphy. The fault zone is distributed, with numerous minor faults breaking the bedded strata. For all three interpreted events, we observed a large number of small faults breaking to a particular level, and then

found to be in stratigraphic order from which we constructed the age model shown in Figure 11. The dates indicate that the entire upper 2.5 m of Big Lake strata were deposited in the past 2600 years, yielding an average sedimentation rate of about a meter per thousand years.

There are two apparent hiatuses or periods of slow deposition, one between units 150 and 190 of about 300 years in length, and one between units 250 and 350 of about 800 years in length. The upper one occurred during the period of accumulation of secondary carbonate in unit 170, and we interpret this to be a generally dry period with little or no sediment deposition during which the secondary carbonate was able to accumulate. The lower hiatus contains unit 300, which we have interpreted as a well-formed buried A or topsoil horizon. It is likely that much of the period of non-deposition is represented by this soil. Periods of non-deposition are potentially significant in that multiple surface ruptures may have occurred for which there is little or no evidence.

In summary, the stratigraphy at Big Lake is reasonably well-stratified and accumulated at a rate of about 1 m/ka, which is a good rate with which to capture paleo-earthquakes. In the

capped by overlying strata. In some cases, faults are observed to break to a level and have an associated filled fissure, which may be rebroken from a subsequent event. For the penultimate event, a scarp formed on a more significant fault strand and was subsequently buried by unbroken strata.

The distributed nature of faulting is consistent with Big Lake being a releasing step-over. Many well-documented historical southern California surface ruptures exhibit similar behavior at releasing steps, as noted for the 1968 Borrego Mountain earthquake (Clark, 1972), the 1987 Superstition Hills earthquake (Sharp et al., 1989), the 1992 Landers earthquake (Sieh et al., 1993), the 1999 Hector Mine earthquake (Treiman et al., 2002), and most recently, the 2010 Cucapah-El Mayor earthquake in northern Baja California (Fletcher et al., 2014). Individual fractures within a step-over may have only minor lateral displacement, and most exhibit opening modes that allow for development of fissures that can be filled with surface sediment.

Event E1 – Event E1 is represented by many small offsets that break up through unit 90 and are capped by unit 50 (Figures 10 and 12). Unit 90 is seen to warp down into fault strands at many locations, and there are filled fissures that we interpret were open cracks resulting from the rupture. Maximum vertical separation on individual faults is on the order of a few centimeters, and there is no significant change in thickness of the overlying unit 50, which suggests that total vertical separation across the entire fault zone is minor or absent.

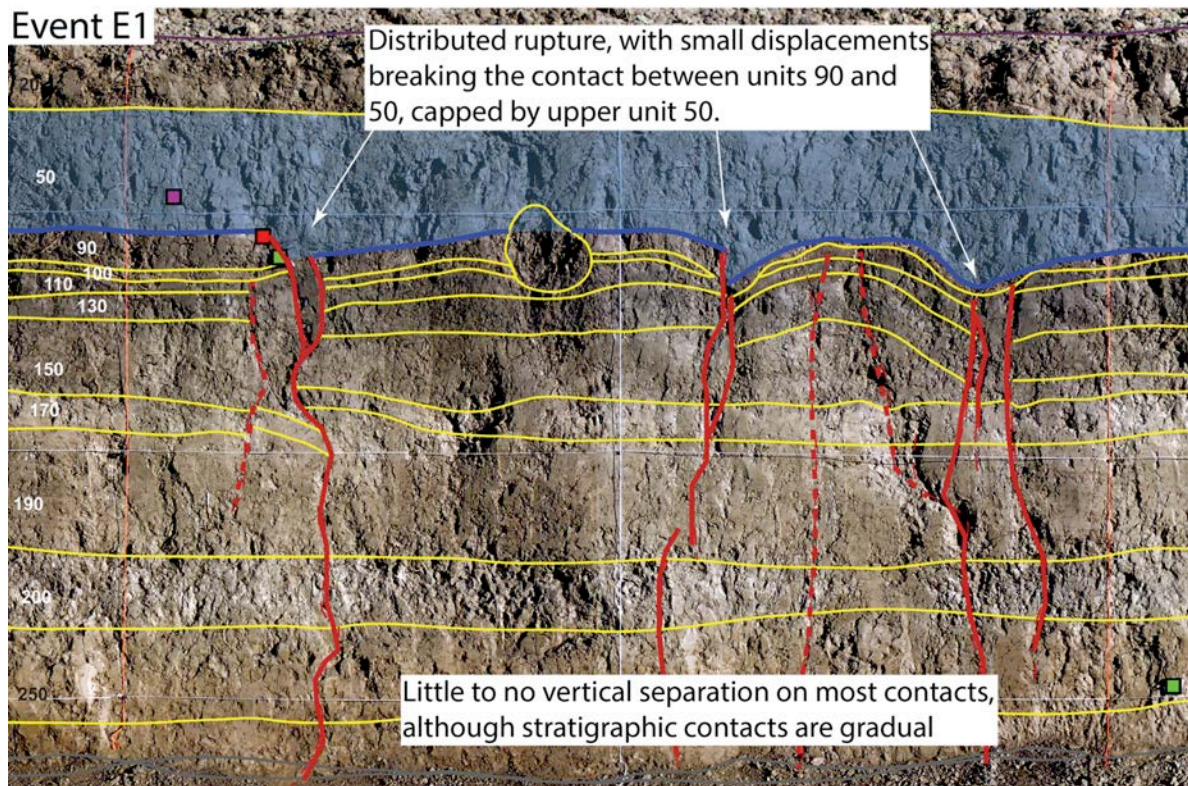


Figure 12. A portion of the NW wall of trench T1 at Big Lake. Many small faults are observed to break up to the top of unit 90 and appear capped by unit 50. Further, there appear to be filled fissures associated with many of these faults that are also capped by unit 50. Based on these observations, the most recent surface rupture is interpreted to have occurred when Unit 90 was at the surface.

The age of event E1 is constrained to be younger than 1810 AD, based on radiocarbon dating (Figure 11). The shotgun shell recovered from the base of unit 20 indicates that deposition has continued into the historical period. These observations suggest that event E1 may be historical in age, which we discuss further in the discussion section.

Event E2 – Rupture interpreted for event E2 is again observed to be distributed across a broad zone (Figure 10), but in this case, there was significant rupture on one of the fault strands, resulting in both significant vertical displacement as well as a mismatch in unit thickness, an indication of significant strike-slip (Figure 13). The rupture breaks up through unit 300 and is capped by unit 280. Unit 300 is interpreted as a buried A horizon and may represent several hundred years of non-deposition. Furthermore, the current age constraints are on units 350 and 250, so the strata that capture the event horizon are not directly dated. Thus, the resulting age constraints on event E2 are poorly constrained to between AD 479 and 1104.

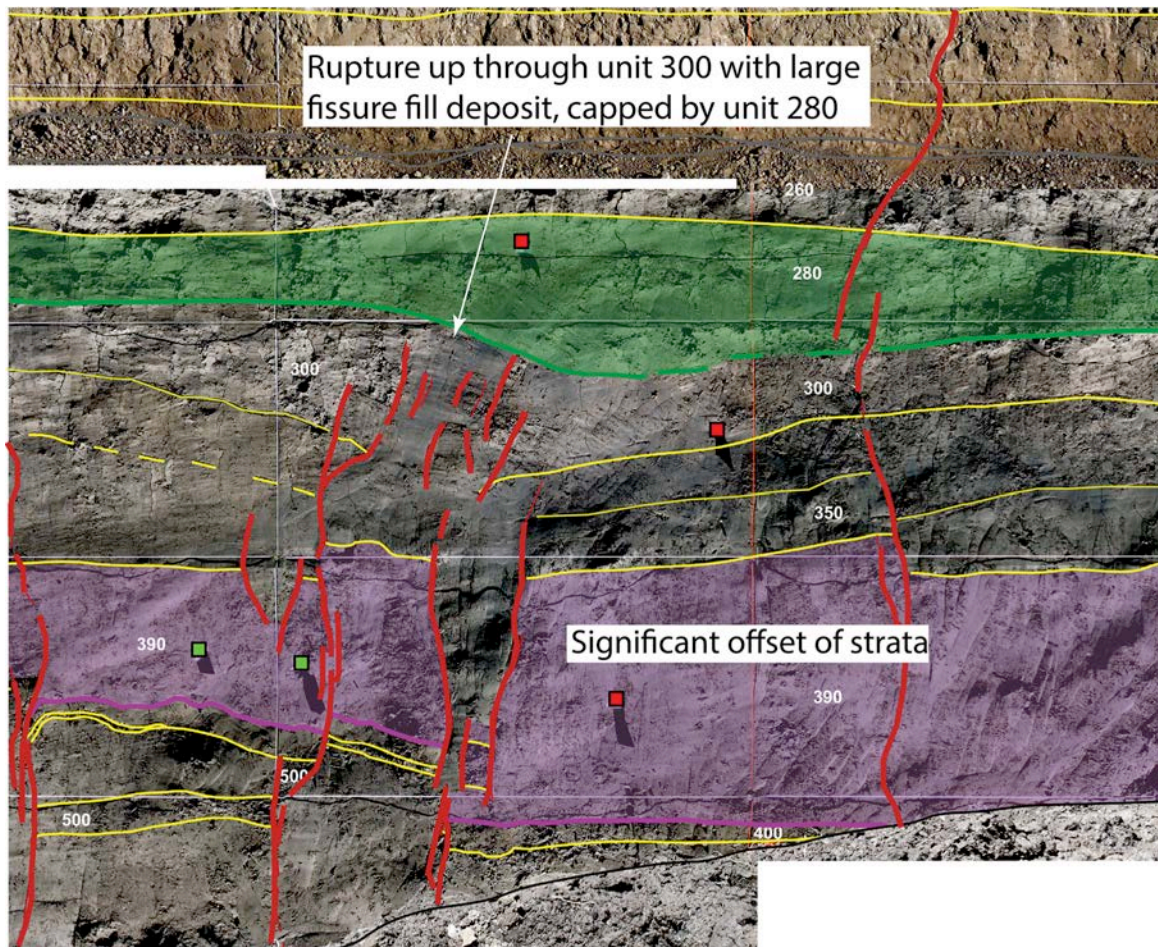


Figure 13. Interpretation of event E2 is based on many faults that disrupt up through unit 300, which we interpret as a buried A horizon, with unit 280 capping the fault. In this figure, units below 300 have significant vertical separations and changes in unit thickness, suggesting significant strike slip occurred in this event. Unit 300 appears fissured down into unit 390, and there is a buried scarp at the top of unit 300, which is buried by unit 280.

Event E3 – Event E3 is represented by numerous small faults with associated filled fissures that break up through unit 420 and are capped by unit 390, and locally unit 400 (Figure 14). Many of these faults exhibit significant vertical separations of strata below unit 390, whereas unit 390 is either unfaulted by these strands, or if rebroken by a later event, commonly exhibits little or no vertical separation. There is an overall down-to-the-northeast sense of vertical displacement for all units below unit 390, with some lower strata dropping below the base of the trench on the northeast side.

The timing of event E3 is moderately well constrained to between BC 166 and AD 204, placing it close to 0 AD. However, two dates are on units 390 and 400, closely post-dating the event, whereas the highest dated stratum below the event horizon is derived from unit 550. Hence, it is likely that the actual age of event E3 lies towards the younger part of the plausible age range.

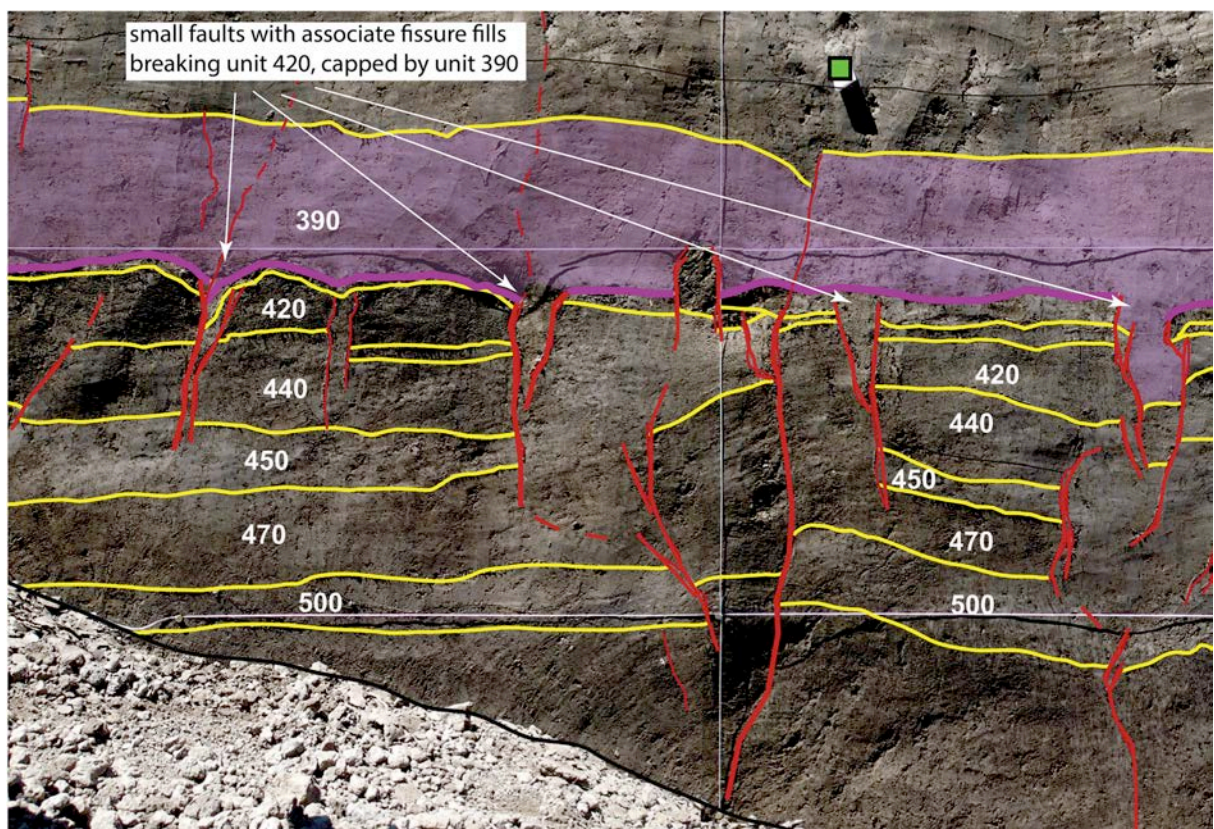


Figure 14. Event E3 is indicated by numerous fault strands that break up through units 420 and are capped by units 390 and 400. Strata below unit 420 show locally significant vertical separations and tilting.

Discussion

We have determined a long-term, mid-Quaternary to present slip rate of about 2.5 mm/yr for the Earthquake Valley fault in Warner Basin. This value is about half of the estimated slip rate along the northern Elsinore fault in the Temecula – Murrieta region (Rockwell et al., 2000), and is similar to the inferred slip rate for the central Elsinore fault southeast of Julian (Magistrale

and Rockwell, 1996). These observations indicate that south of the Agua Tibia-Palomar Mountain uplift, the slip rate is evenly divided between the Elsinore and Earthquake Valley faults. As the Earthquake Valley fault appears to transfer its slip southeastward to the San Jacinto fault via a restraining step at the Vallecitos-Fish Creek Mountain uplift, this may explain why Fialko (2006) attributed nearly 20 mm/yr to the southern San Jacinto fault, a rate that is similar to that attributed to the southern San Andreas fault. In our model, about 2.5 mm/yr of the Elsinore slip rate is added to the ~14 mm/yr documented for the central San Jacinto fault (Blisniuk et al., 2013), with likely some additional rate distributed among the northeast-striking left-lateral cross faults. This implies that the San Jacinto fault remains subordinate to the southern San Andreas fault in terms of slip on discrete faults.

The recurrence interval that we have determined for the Earthquake Valley fault at Big Lake is on the order of about 800-1000 years. This is based on the occurrence of an event at about 0 AD, one at about 800 AD (between 479 and 1104 AD), and one in the past two hundred years. The penultimate two events appear to have produced significantly more vertical separation than the MRE so they may have been larger, although with strike-slip faults, this type of inference can be wrong. For an estimate of displacement, we assume that each event was similar in size and we also assume that three events are sufficient to accurately represent the average recurrence interval. This last assumption is commonly wrong, as long paleoseismic records almost always show some periods of increased or decreased seismic activity (Rockwell et al., 2014). Nevertheless, if the average recurrence interval is about 900 years, a 2.5 mm/yr slip rate suggests that displacement per event should be on the order of 2.2 m. This value is larger than likely occurred in the 1890 earthquake, as discussed below, which argues in contrast that the MRE was smaller than the prior two events.

Is the MRE at Big Lake an historical earthquake? - Event E1 is very young and almost certainly historical in age, although the historical record is incomplete for moderately large earthquakes prior to about 1850. There are two plausible moderately large earthquakes that do generally fit a rupture along the earthquake Valley fault, the 9 February 1890 and 28 May 1892 earthquakes. The 1890 earthquake is reported from Yuma, Los Angeles and San Diego at MMI V, whereas the 1892 earthquake is reported as MMI IV from Los Angeles and MMI V for San Diego and Yuma (Figure 15). Toppozada et al. (1981) suggest a magnitude of about M6.5 for each of these events, although the instrumentally reported 25 December 1899 earthquake on the

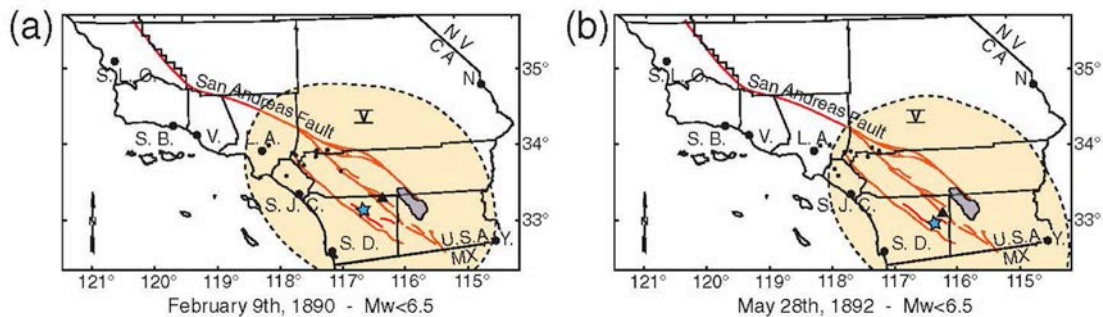


Figure 15. *Isoseisms for the 1890 and 1892 earthquakes (from Toppozada et al., 1981). The triangles are the locations suggested by Toppozada et al., whereas the stars are along the Earthquake Valley fault.*

San Jacinto fault near Hemet produced MMI V for a slightly greater region and that earthquake is fairly well established at about Mw6.5 (Ellsworth, 1990), so the 1890 and 1892 earthquakes were probably slightly smaller. Topozada et al. (1981) tentatively placed these earthquakes along the south-central San Jacinto fault due to lack of local control, and because the San Jacinto fault is a major fault and likely source for such events. However, Salisbury et al. (2012) show that the most recent surface rupture along the Clark strand of the fault is likely the November 22, 1800 earthquake, and the displacements, which reach a maximum value near Anza of 3-4 m, argues that this event is significantly larger than either the 1890 or 1892 earthquakes. An earthquake of M6.3-M6.4 is large enough to rupture the surface in southern California, but it is close to the minimum size with reported surface rupture. Minor distributed displacement for the most recent event at Big Lake is consistent with the sizes of the 1890 and 1892 earthquakes, and we suggest the possibility that one of these events produced the surface cracking that we observe at Big Lake. If correct, then the other moderate event may have also been along the Earthquake Valley fault, and most likely to the south as a northern rupture should have produced more damage at Los Angeles than in San Diego or Yuma. That would suggest that the 1890 event is the northern of the two, consistent with the lesser damage reported at Los Angeles in 1892 (Topozada et al., 1981).

If we are correct that 1890 and/or 1892 earthquakes produced rupture on the Earthquake Valley fault, this has significant implications as to the degree that the M7.3 El Mayor-Cucapah earthquake may have brought the southern Elsinore fault system closer to failure. Rockwell (1990, and unpublished data) demonstrated that the southernmost strand of the Elsinore fault failed in a relatively large earthquake sometime after AD 1680, with maximum slip in the Coyote Mountains measured at 2.7 m. The

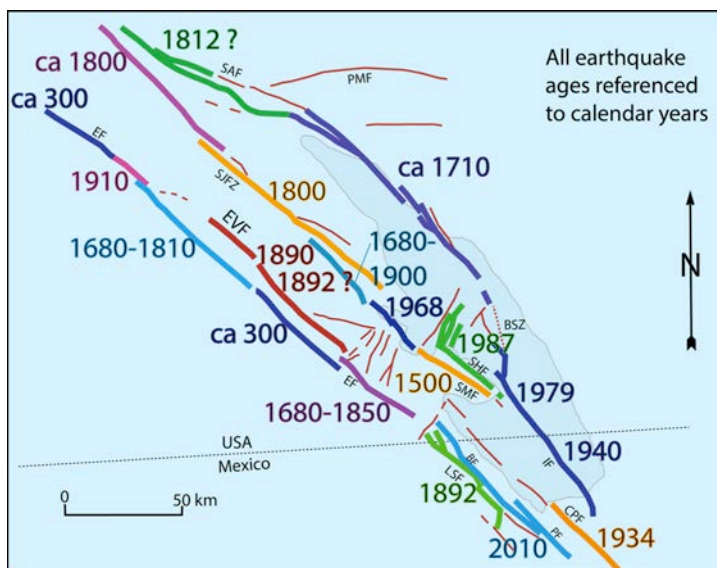


Figure 16. Timing of the most recent surface rupture on faults of the southern San Andreas fault system. In this figure, we assume that that event E1 identified at Big Lake is the 1890 earthquake. Note that the southernmost Elsinore fault in the Coyote Mountains has sustained a recent rupture, as has the Laguna Salada fault, which ruptured in 1892.

minimum rupture length is estimated at 40 km, which when combined with the displacement, suggests an earthquake in the Mw6.9 range. This observed displacement is too large to fit either 1890 or 1892, or any other known historical earthquake, so it probably occurred prior to construction of the San Diego mission in 1769. This implies that the southernmost Elsinore fault in the Coyote Mountains was first to fail, followed by an earthquake on the Earthquake Valley fault in 1890, the Laguna Salada fault in February of 1892, and a second shock on the Earthquake Valley fault in May 1892 (Figure 16). If correct, and if the estimated recurrence interval for the southern Elsinore fault of about 1 ka is correct, then the 2010 earthquake is

unlikely to have sufficiently loaded either the Elsinore or Earthquake Valley faults to produce failure in the near future. In contrast, the most recent surface rupture on the southernmost part of the San Jacinto fault – the Superstition Mountain strand, has not failed in nearly 500 years, making it one of the ripest faults in the southern San Andreas system, although the 2010 earthquake did little to load this strand.

Conclusions

The Earthquake Valley fault has a slip rate of $2.5^{+0.3}/_{-0.5}$ mm/yr, as determined by 1.9 km offset of the Warner Basin alluvial fill deposits which contain the ~780 ka Bishop Tuff. The fault has produced three surface ruptures in the past 2 ka at Big Lake, with the MRE possibly the 1890 earthquake reported for this region by Topozada et al. (1981), suggesting a recurrence interval in the range of 800-1000 years. As the fault has experienced a recent rupture, it is not likely to produce another large earthquake in the near future.

References Cited:

- Blisnuik, K., M. Oskin, A-S. Mériaux, T. Rockwell, R. Finkel, and F. J. Ryerson (2013). Stable, Rapid Rate of Slip Since Inception of the San Jacinto Fault, California, *Geophys. Res. Ltr.*, **40** 4209–4213.
- Chamberlain, K. J., Wilson, C. J. N., Wooden, J. L., Charlier, B. L. A., & Ireland, T. R. (2013). New perspectives on the Bishop Tuff from zircon textures, ages and trace elements. *Journal of Petrology*, **55** (2), 395-426.
- Clark M.M. (1972) Surface rupture along the Coyote Creek fault. U.S. Geol. Survey Prof. Pap. 787, 55-86.
- Ellsworth, W. L. (1990). Earthquake history, 1769–1989, in *The San Andreas Fault System, California*. R. E. Wallace (Editor), U.S. Geol. Surv. Profess. Pap. 1515, chap. 6, 152–187.
- Fialko, Y. (2006). Interseismic strain accumulation and the earthquake potential on the southern San Andreas fault system. *Nature* **441** 968–971, doi:10.1038/nature04797.
- Fletcher, K.E.K., Rockwell, T.K., and Sharp, W.D. (2011). Late Quaternary slip rate of the southern Elsinore fault, southern California: Dating offset landforms via ²³⁰Th/U on pedogenic carbonate. *Journal of Geophysical Research*, **116** F02006, doi:10.1029/2010JF001701.
- Fletcher, J.M., O. J. Teran, T. K. Rockwell, M. Oskin, K. W. Hudnut, K.I J. Mueller, R. M. Spelz, S. O. Akciz, E. Masana, G. Faneros, A. Morellan, J. Stock, A. Elliott, P. Gold, J. Liu-Zeng, A. Gonzalez, D. Lynch, A. Hinojosa, J. Gonzalez (2014). Assembly of a large earthquake from a complex fault system: surface rupture

- kinematics of the April 4, 2010 El Mayor-Cucapah Mw7.2 earthquake. *Geosphere*, **10** (4) 797-827.
- Magistrale, H. and T. Rockwell (1996). The central and southern Elsinore fault zone, southern California: *Bulletin of Seismological Society of America*, **86** 1793-1803.
- Merriam, R. & Bischoff, J.L. (1975). Bishop ash – A widespread volcanic ash extended to southern California: *Journal of Sedimentary Petrology*, **45** (1) 207-211.
- Paces, J. B., & Miller, J. D. (1993). Precise U-Pb ages of Duluth Complex and related mafic intrusions, northeastern Minnesota: Geochronological insights to physical, petrogenetic, paleomagnetic, and tectonomagmatic processes associated with the 1.1 Ga Midcontinent Rift System. *J. Geophysical Research: Solid Earth* **98** (B8) 13997-14013.
- Reid, M. R. and C. D. Coath (2000). In situ U-Pb ages of zircons from the Bishop Tuff: No evidence for long crystal residence times. *Geology*, **28** (5) 443-446.
- Rivera, T. A., M. Storey, C. Zeeden, F. J. Hilgen, and K. Kuiper (2011). A refined astronomically calibrated $^{40}\text{Ar}/^{39}\text{Ar}$ age for Fish Canyon sanidine. *Earth and Planetary Science Letters*, **311** (3) 420-426.
- Rockwell, T., M. Bergmann, and M. Kenney (2000). Holocene slip rate of the Elsinore fault in Temecula Valley, Riverside County, California. In *Geology and Enology of the Temecula Valley* (B. Birnbaum and K. Cato, eds), 105-118.
- Rockwell, T.K., T.E. Dawson, J. Young-Ben Horton, and G. Seitz (2014 in press). A 21 event, 4,000-year history of surface ruptures in the Anza Seismic Gap, San Jacinto Fault and implications for long-term earthquake production on a major plate boundary fault. Accepted to *Pure and Applied Geophysics*, June, 2014.
- Rymer, M.J., and 14 others (2011). Triggered surface slips in southern California associated with the 2010 El Mayor–Cucapah, Baja California, Mexico, earthquake: U.S. Geological Survey Open-File Report 2010–133, 62 p.
- Salisbury, J.B., T.K. Rockwell, T.J. Middleton, and K.W. Hudnut (2012). LiDAR and Field Observations of Slip Distribution for the Most Recent Surface Ruptures Along the Central San Jacinto Fault. *Bull. Seismo. Soc. Am.*, **102** (2) 598-619.
- Schmitt, A. K. and J. B. Hulen (2008). Buried rhyolites within the active, high-temperature Salton Sea geothermal system. *J. Volcanology and Geothermal Research*, **178** (4), 708-718.
- Schmitt, A. K., M. Grove, T. M. Harrison, O. Lovera, J. Hulen, and M. Walters (2003). The Geysers-Cobb Mountain Magma System, California (Part 2): timescales of

pluton emplacement and implications for its thermal history. *Geochimica et Cosmochimica Acta*, **67** (18), 3443-3458.

Sharp, R. V., K. E. Budding, J. Boatwright, M. J. Ader, M. G. Ader, M. G. Bonilla, M. M. Clark, T. E. Fumal, K. K. Harms, J. J. Lienkaemper, D. M. Horton, B. J. O'Neill, C. L. Ortergren, D. J. Ponti, M. J. Rymer, J. L. Saxton, and J. D. Sims (1989). Surface faulting along the Superstition Hills Fault Zone and nearby faults associated with the earthquakes of 24 November 1987, *Bull. Seismol. Soc. Am.* **79** 252–281.

Sieh, K., L. Jones, E. Hauksson, K. Hudnut, D. Eberhart-Phillips, T. Heaton, S. Hough, K. Hutton, H. Kanamori, A. Lilje, S. Lindrall, S. McGill, J. Mori, C. Rubin, J. Spotila, J. Stock, H. K. Thio, J. Treiman, B. Wernicke, and J. Zachariasen (1993). Near-field investigations of the Landers earthquake sequence, April to July, 1992, *Science* **260** 171–176.

Simon, J. I., & Reid, M. R. (2005). The pace of rhyolite differentiation and storage in an 'archetypical' silicic magma system, Long Valley, California. *Earth and Planetary Science Letters*, **235** (1) 123-140.

Simon, J. I., Weis, D., DePaolo, D. J., Renne, P. R., Mundil, R., & Schmitt, A. K. (2014). Assimilation of preexisting Pleistocene intrusions at Long Valley by periodic magma recharge accelerates rhyolite generation: rethinking the remelting model. *Contributions to Mineralogy and Petrology*, **167** (1) 1-34.

Toppazada, T., C. Real, and D. Parke (1981). Preparation of isoseismal maps and summaries of reported effects for pre-1900 California earthquakes, California Division of Mines and Geology Open-File Rept. 81-11 SAC, 182 p.

Treiman, J.A., K.J. Kendrick, W.A. Bryant, T.K. Rockwell, S.F. McGill (2002) Primary surface rupture associated with the Mw7.1 16 October 1999 Hector Mine earthquake, San Bernardino County, California. *Bull. Seismo. Soc. Am.* **92** (4) 1171-1191.